CHALMERS
UNIVERSITY OF TECHNOLOGY

Detection of alkali path in a pilot-scale combustor using laser spectroscopy and surface ionization — From vapor to particles

Fuel 343 (2023) 127900

Contents lists available at ScienceDirect

Fuel

journal homepage: www.elsevier.com/locate/fuel

Full Length Article

Detection of alkali path in a pilot-scale combustor using laser spectroscopy and surface ionization — From vapor to particles

Jan Viljanen [a,b,*], Dan Gall [b], Ivan Gogolev [b], Thomas Allgurén [b], Klas Andersson [b]

[a] Photonics Laboratory, Physics Unit, Tampere University, Tampere, 33101, Finland
[b] Department of Space Earth & Environment, Chalmers University of Technology, Gothenburg, 412 96, Sweden

ARTICLE INFO

Keywords:
Diagnostics
Potassium
Alkali
Sulfation
Nucleation

ABSTRACT

Alkali species have been under intensive research in thermal conversion applications due to their abundance especially in biomass fuels. Alkali metals, sodium (Na) and potassium (K), are known to cause severe operational problems in combustion units, such as slagging, fouling, and corrosion. In this work, we present a monitoring method to follow alkali behavior from vapor to particles in a pilot-scale reactor. In our approach we combine Tunable Diode Laser Atomic Spectroscopy (TDLAS) for atomic potassium monitoring, Collinear Photofragmentation and Atomic Absorption Spectroscopy (CPFAAS) for KCl and KOH detection, and Surface Ionization Detection (SID) for monitoring of total flue gas and aerosol alkali content. Experiments were carried out in the Chalmers 100 kW oxy-fuel combustion unit that, during these experiments, used propane as fuel. Alkali species were injected as a water solution directly to the flame. In addition, SO_2 was used to alter the conditions for alkali species formation injecting it directly to the combustion feed gas. Due to the alkali monitoring system described, we were able to monitor the alkali behavior during nucleation and sulfation processes. The conditions for dimer formation and heterogeneous nucleation were observed when the temperature conditions were changed by lowering the thermal input to the unit.

1. Introduction

Interest in alkali element behavior in high-temperature environments has remained high due to their abundance in biomass and waste-derived fuels and, on the other hand, due to large high-alkali-content coal reserves, such as the Zhundong coal reserve [1,2]. Alkali metals, especially sodium (Na) and potassium (K), are known to cause severe operational problems in the combustion units, such as slagging, fouling, and corrosion. The alkali elements may also interfere with the combustion process itself by promoting or inhibiting the fuel oxidation, depending on the prevailing conditions [3,4]. In addition to the combustion conditions, the intensity and direction of the alkali related effects depend on the molecular form that the alkali elements are present in the process gases and on the combustion unit surfaces. From corrosion perspective, the most problematic forms of alkali elements are alkali chlorides: KCl and NaCl. These alkali species induce high corrosion rates on the heat transfer surfaces. To mitigate the adverse effects, the temperature on heat transfer surfaces is lowered, hence, making the alkali species one of the main reasons for lowered efficiency of biomass and waste-fired power plants when compared to coal-fired plants [5].

The main alkali vapor species during the combustion process are alkali chlorides, hydroxides, and sulfates that are formed through complicated series of reactions. If chlorine is available, the alkali elements are released from the fuel as chlorides. Otherwise they are usually released as atomic species or as hydroxides [6]. In fuel-rich conditions, the main in-flame alkali species are the atomic species [7]. When the alkali species enter the post-flame region, they form chlorides and hydroxides that can be further sulfated if sulfur and suitable conditions are available [8]. In addition to gas phase reactions, alkali species may take part on number of processes, such as homogeneous nucleation, coagulation, and heterogeneous condensation, that result in alkali containing aerosols. The resulting alkali-rich particulate matter can onset the deposit growth on heat exchanger surfaces leading to formation of corrosive ash deposits [9]. By simulations and laboratory experiments, the nucleation temperature of chlorides have been found to be at around 700 °C [10,11]. Formation of particulate matter can be dramatically increased when sulfation occurs as the sulfates become quickly supersaturated due to the lower vapor pressure [10,12]. Therefore, the alkali content in solid phase is highly relevant, especially, for evaluation of alkali behavior in flue gases resulting from biomass and oxy-fuel applications. Thus, to obtain full picture of the alkali

* Corresponding author at: Photonics Laboratory, Physics Unit, Tampere University, Tampere, 33101, Finland.
E-mail address: jan.viljanen@tuni.fi (J. Viljanen).

https://doi.org/10.1016/j.fuel.2023.127900
Received 15 December 2022; Received in revised form 9 February 2023; Accepted 17 February 2023
Available online 24 February 2023

species concentration, their behavior, and possible adverse effects on the unit operation, the alkali species concentration in gas and solid phase must be monitored simultaneously. Therefore, complementing alkali diagnostic methods are required.

The main challenge on understanding the potassium dynamics in industrial-scale systems has been the lack of adequate alkali diagnostics. Despite the increasing number of alkali analysis techniques, the harsh environment in large-scale units has been limiting the alkali analysis mostly into bench-scale reactors. Laser diagnostic tools for alkali species have been utilized extensively in high-temperature gases and some of the laser-based techniques have been demonstrated also in industrial scale [13]. For example, Tunable Laser Absorption Spectroscopy (TDLAS) [14,15], that is a mature technique for atomic potassium quantification, and Ultraviolet Differential Optical Absorption Spectroscopy (UV-DOAS) [16], developed for molecular alkali species diagnostics, have been in use for industrial-scale alkali monitoring. A laser-based technique called Collinear Photofragmentation and Atomic Absorption (CPFAAS) [17] has been demonstrated for molecule specific KCl and KOH detection in industrial-scale units [18]. In addition, the photofragmentation-based technique was recently combined with TDLAS making it capable to simultaneously detect K, KCl and KOH in a flame and in a flue gas stream [7]. The combination of photofragmentation and TDLAS has also been demonstrated in a pilot-scale entrained flow gasifier unit [19]. However, the detection ability of molecule selective laser-based methods is limited to selected alkali species in gas phase.

In this work, we demonstrate an experimental method to follow alkali species during combustion – from vapor to particles – that would enable the alkali path monitoring and determination of the fractions of alkali species in the flue gas and in the particles in varying conditions. The CPFAAS method is combined with TDLAS to enable simultaneous monitoring of K, KCl and KOH fractions in the gas phase in the transition region from the in-flame to the post-flame conditions and in the flue gas. We complement the species-specific laser diagnostic alkali information with the use of a Surface Ionization Detector (SID) [20] that is capable of monitoring the total alkali concentration, i.e. both gas and solid phase, in the flue gas [21,22]. The information obtained with the two independent methods are compared and combined to form a more complete picture of the alkali path through the system. It is demonstrated that adjacent monitoring methods are required for alkali monitoring especially in dynamic combustion conditions with load-ramping and varying fuel and additive qualities and quantities. The possibilities and limitations of the adjacent measurement systems are explored and discussed. The experiments are carried out in the 100 kW Chalmers Oxy-fuel reactor that is a combustion unit capable of different combustion conditions and rapid condition shifts. The unit is equipped with multiple optical access points along the combustion axis enabling laser diagnostics along the reactor axis. The laser-based diagnostic system is demonstrated to be able to monitor potassium species in different combustion environments, including oxy-fuel environment (high CO_2 and SO_2 concentrations) and the response of different potassium species to SO_2 injection is investigated in different distances from the burner.

2. Experimental arrangement

2.1. Combustion unit

The experiments were carried out in the Chalmers 100 kW oxy-fuel unit [23,24]. The unit has an inner height and diameter of 2400 mm and 800 mm, respectively, as shown in Fig. 1. The unit is equipped with measurement ports at seven different distances along the suspended flame axis on four sides of the cylindrical unit. In addition, there is an eighth measurement position in the flue gas exit. In this work, the unit was operated with propane as the fuel with, in most cases, a feeding rate of 1.73 g/s (80 kW) and a stoichiometric oxygen-to-fuel ratio of 1.15. The unit was operated in two different conditions: air combustion (Air) and oxy-fuel condition. During the oxy-fuel operation, the combustion air was replaced with dry recirculated flue gas to which oxygen was added to reach a concentration of 25% of oxygen in the combustion gas (OF25). The main components in the resulting flue gas are presented for both cases in Table 1. The facility has the possibility to add gaseous species into the combustion air or into the recirculated flue gas. In this work, this system is used to inject SO_2. The injection flow is controlled using a mass flow controller set to reach different flue gas concentrations. The theoretical SO_2 concentrations in flue gas in the different combustion and injection cases are presented in Table 1. In addition, the unit has a system for spray injection of aqueous solutions directly into the flame. The spray nozzle has a spray angle of 15° and is located 40 mm below the burner. This spray system was used to inject aqueous solutions containing KCl and NaCl into the flame. The water solution flow is controlled with a peristaltic pump (Prominent, DELTA 1612) with flow rate set to 0.9 lph. The flow rate was held constant throughout the experiments. The concentration of injected species was altered by changing the alkali concentration in the solution aiming at flue gas alkali concentrations of 10 ppm, 50 ppm, and 100 ppm.

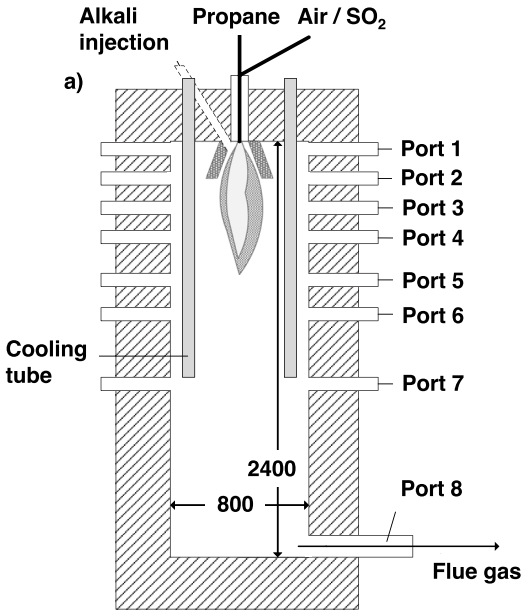

Fig. 1. Schematic presentation of the Chalmers 100 kW oxy-fuel unit. The reactor has measurement ports on all four sides on all levels marked with Port 1–8.

Table 1
The main combustion gas concentrations in different combustion cases and theoretical maximum SO_2 concentrations during two different injection levels.

	Air	OF25
Thermal input (kW)	80	80
Oxygen-to-fuel ratio	1.15	1.15
O_2	2.6	3.0
CO_2	10.2	81.0
H_2O	13.6	16
Residence time (s)	4.4	5.6
SO_2 injection low/high (ppm)	300/600	975/2300

2.2. Gas composition and temperature measurements

The gas composition was measured using a temperature-controlled sampling system. In this system the hot gases are sampled using a water-cooled probe with a 6 mm electrically heated center pipe through which the gas is extracted. The center pipe is heated to 180 °C to avoid condensation. The probe is connected to an FTIR (MultiGas 2030, MKS Instrument Inc.) and a paramagnetic oxygen analyzer via a fully heated

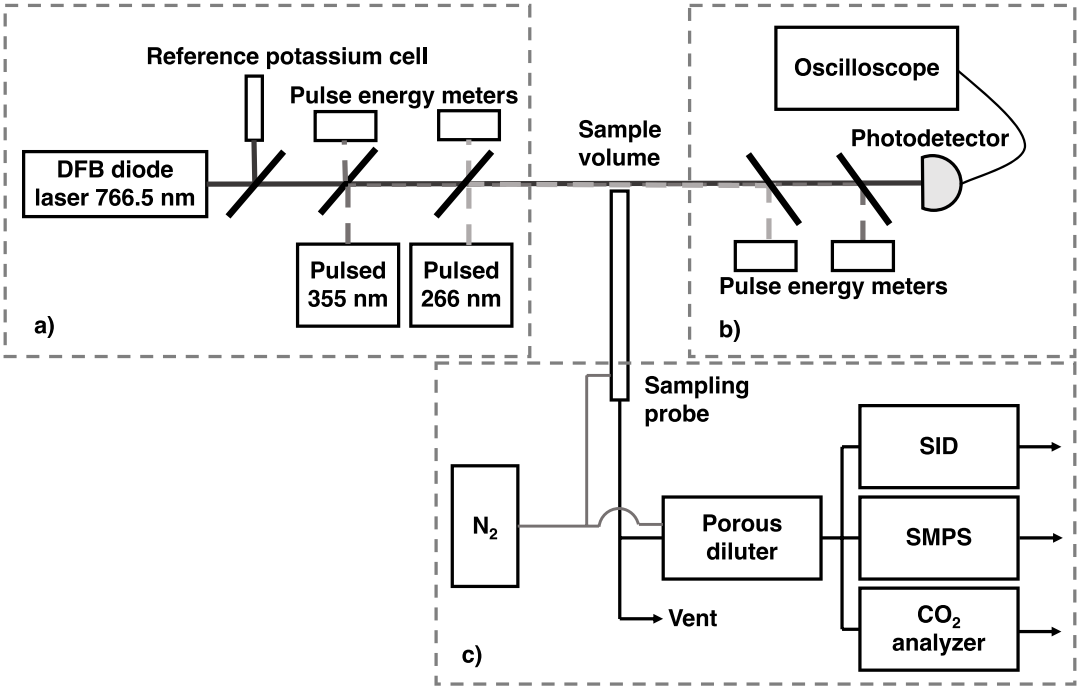

Fig. 2. Schematic of the (a) CPFAAS+TDLAS arrangement and (b) the SID sampling and dilution arrangement. The beam path was aligned through the reactor center and the SID sampling probe was placed 3 cm away from the beam path in Port 7.

sampling line, including heated filters and pumps, all set to 180 °C. The FTIR is used to detect several different components, such as H_2O, CO_2, SO_2, and HCl. During oxy-fuel combustion, an additional CO_2 analyzer (NGA 2000) was used to obtain calibrated CO_2 values up to 100% concentration. The temperature is determined using a suction pyrometer equipped with a thermocouple type B. The thermocouple is shielded using a ceramic tube through which the hot gas is sucked.

2.3. Laser diagnostic arrangement

Potassium species K, KCl, and KOH were monitored in gas phase using in-situ laser technique called CPFAAS that was equipped with tunable laser diode for TDLAS. The laser measurement arrangement is shown in Fig. 2. Atomic potassium concentration is monitored using distributed feedback (DFB) diode laser (Nanoplus GmbH) that is wavelength modulated across potassium D2 line at 766 nm. The temporal beam transmission through the center of the combustion unit is monitored using a photodetector (PDA10A, Thorlabs Inc) that is connected to a spectrometer (HDO6054, LeCroy). A reference potassium cell (SC-K-19375-Q-W, Photonics Technologies) is used to monitor and validate the atomic potassium probe beam wavelength. Two photofragmenting laser pulses are synchronized with the potassium probe wavelength modulation and aligned collinearly with the potassium probe beam enabling the detection of atomic potassium fragments produced by the laser pulses. The first laser pulse is emitted at wavelength of 355 nm. It has a temporal width of 5 ns and a furnace input pulse energy of 800 μJ (Ultra Big Sky series, Quantel). The second laser pulse is emitted at wavelength of 266 nm, with a temporal width of 1 ns, and a furnace input pulse energy of 20 μJ (FQSS-266-200, CryLas GmBh). The temporal separation of the laser pulses is long enough (>100 μs) to allow the transmission signal to recover after the initial photofragmentation. The laser pulse at 355 nm dissociates KOH whereas the laser pulse at 266 nm dissociates both KCl and KOH. Thus, the contribution of atomic potassium originating from KOH during the laser pulse at 266 nm can be subtracted using the information obtained during the laser pulse at 355 nm [25]. The laser beams were aligned through the combustion unit utilizing the measurement ports described in Section 2.1. The ports were equipped with sapphire glass windows and flushed with N_2 flow.

The precursor molecule concentration X_{prec} is obtained by using Eq. (1) that consider extinction of the fragmenting laser pulse when it propagates through the measurement volume [26].

$$X_{prec} = \alpha L_{\max} \frac{A_f}{E_{in} L} \frac{hc}{\gamma \lambda_f} \frac{kT}{p} \frac{1}{\sigma_K(\nu)\sigma_{prec}} \frac{\ln\left(\frac{E_{in}}{E_{out}}\right)}{1 - \frac{E_{out}}{E_{in}}}, \quad (1)$$

where αL_{max} is the maximum increase in the probe beam absorptivity after the fragmenting laser pulse, A_f is the area of the fragmenting beam, E_{in} is the energy of the fragmentation laser pulse at the furnace input, L is the interaction length of the beams and the sample, i.e. in this case, the unit diameter, h is the Planck's constant, c is the speed of light, γ is the photofragmentation efficiency, λ_f is the fragmentation wavelength, k is the Boltzmann's constant, T is the sample temperature, p is the sample pressure, $\sigma_K(\nu)$ is the wavelength dependent absorption cross section of atomic potassium, σ_{prec} is the absorption cross section of corresponding precursor molecule, and E_{out} is the energy of the fragmentation laser pulse at the furnace output [26]. The photofragmentation efficiency is assumed to be unity for both KCl and KOH. The aL_{max} is obtained using exponential fitting double exponential curve to the obtained temporal absorbance signal [27]. The $\sigma_K(\nu)$ value at the time of the fragmentation and subsequent aL_{max} measurement is determined by comparing the temporal relation of the fragmenting laser pulse and the tuning of the potassium probe laser wavelength [7]. The absorption cross section values for fragmenting laser pulses used in this work are $\sigma_{KCl,266} = 0.74 \times 10^{-21}$ m^2, $\sigma_{KOH,355} = 0.15 \times 10^{-21}$ m^2 and $\sigma_{KOH,266} = 0.1 \times 10^{-21}$ m^2 [18]. Thus, the limit of detection (LoD) for the single shot detection of KCl and KOH were 1 ppm and 0.05 ppm, respectively.

The atomic potassium concentration along the line-of-sight can be obtained utilizing the Beer–Lambert's law

$$I(\nu) = I_c + I_0(\nu)\exp[-\alpha(\nu)L], \quad (2)$$

where $I(\nu)$ is the intensity of the observed transmitted light, I_c is the frequency-independent part of the laser light intensity, $I_0(\nu)$ is the frequency-dependent intensity of the light inserted to the measurement volume, $\alpha(\nu)$ is the frequency-dependent absorbance that occurs along

the light propagation path, and L is the interaction length of the sample and the light [14]. To obtain $I_0(\nu)$, the transmission intensity through empty furnace was measured before and after the day of measurements and between the change of solutions when pure water was injected to the unit through the peristaltic pump. A Voigt curve was used as fitting to obtain the temperature-dependent potassium absorption lineshape from the measured signal.

2.4. Surface Ionization Detector (SID)

The total alkali concentration in gas phase and in particles was monitored using a SID. It is an online measurement method that draws flue gas from the sampling zone, dilutes the sample gas, and cools it down. The primary particles, i.e., the particles formed prior the sampling, combine with condensing alkali components and impact on a hot platinum filament that is positioned across the sample flow. The particles impinging the filament melt and undergo a phenomenon referred to as surface ionization [28,29]. The platinum filament is charged with a positive voltage causing a strong repelling force to the created K+ and Na+ cations. The cations draw a current upon collection to a detector plate that can be correlated to the total alkali concentration in the sample flow. To obtain the alkali mass concentration (mg/m^3) corresponding to the observed ion current, reference measurements were performed using known mass loadings of synthesized alkali particles [30]. In addition to SID analysis, the particle size distribution is monitored using scanning mobility particle sizer (SMPS) system (TSI 3082) consisting of a differential mobility analyzer (TSI 3081) and a condensation particle counter (TSI 3750) using a soft neutralizer (TSI 3088). The schematic of the dilution and sample extraction arrangement is shown in Fig. 2. The calibration particles were generated using a constant output atomizer (TSI 3076). The calibration was performed using alkali salts KCl, K2SO4, KNO3, and KOH. Detailed description of the calibration can be found in Ref. [30].

The extraction and conditioning of the sample gas is performed using a temperature-controlled probe which enable extraction from the reactor region of interest. In this work, sample gas was extracted from measurement Port 7 that is in the region where particle nucleation can be observed for various conditions. As SID method is incapable to distinguish between alkali species present in gas phase or solid phase, this region serves as an ideal region to compare in-situ laser diagnostics and SID alkali monitoring. The probe has several openings around the inlet to enable fast and efficient dilution and quenching of the sample. The overflow of the dilution gas cools the sample rapidly creating aerodynamic quenching [31]. To examine the amount of deposition losses in the probe line, the probe was rinsed with purified water before and after each day. The probe rinse was diluted 20 times and analyzed with inductively coupled plasma mass spectrometry (ICP–MS, Thermo iCAP Q), and signal intensities for elemental mass were analyzed with ICP–MS (Thermo iCAP Q) and inductively coupled plasma optical emission spectrometry (ICP–OES, Thermo iCAP 6500) for elements in the ppb and parts per million (ppm) ranges, respectively. The sampling losses were found to be insignificant to the resulted alkali concentrations [30]. To determine the dilution ratio, CO_2 levels of the diluted sample was measured (LI-COR LI-850) and compared to the CO_2 measurements of the undiluted gas. The undiluted CO_2 concentration was measured with a Fourier transform infrared spectroscopy (MKS MGS3000) extracted downstream of Port 7.

3. Results and discussion

3.1. Combustion unit temperature profiles

The temperature profile of the unit is measured with suction pyrometry. The temperature during air combustion reaches the maximum temperature of 1750 °C in Port 2 and thereafter decrease to about 800 °C in Port 7. There was no notable difference in temperature between the different injection liquids. The temperatures in Fig. 3 are from the air combustion case with pure water injection. The obtained temperature profile between ports 2 and 7 during air combustion is presented in Fig. 3a that was obtained by measuring point-wise temperature at seven different distances from the unit wall at each port level and using linear interpolation between the measured temperature values. The temperature at Port 7 was found to be dominated by the unit wall temperature and, thus, it was very similar in both combustion cases. The temperature profiles in Port 6 varied between the cases and are presented in Fig. 3b. In case of air combustion, the visual flame tip was observed to fluctuate between Port 5 and Port 6. In case OF25 condition the visual flame was shorter. The differences in the temperature profile and in the flame length are important for the interpretation of the gas phase alkali results.

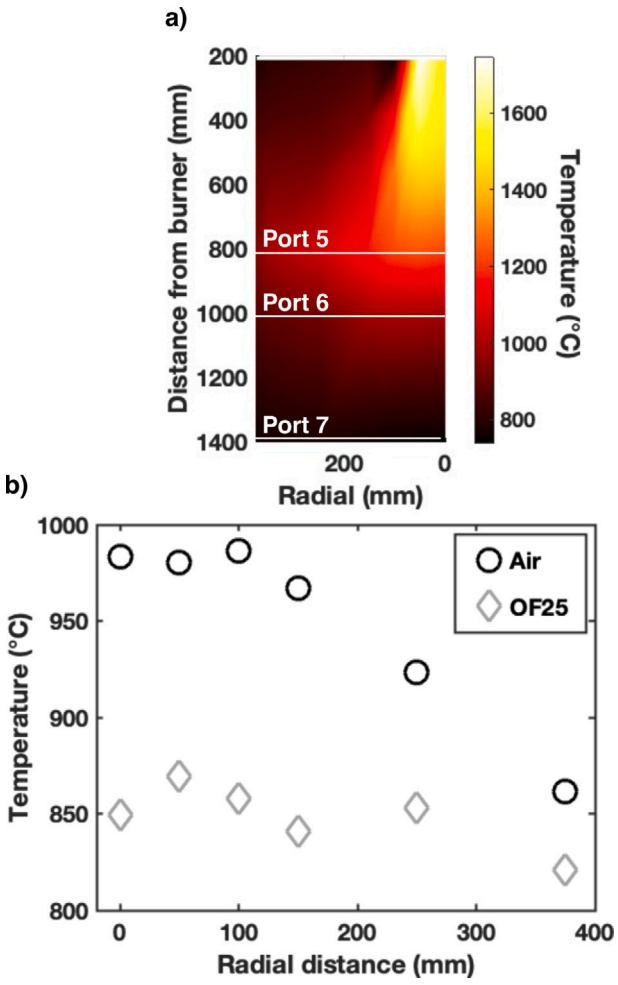

Fig. 3. (a) The temperature profile between Ports 2 and 7 of the combustion unit during air combustion. (b) The radial temperature at Port 6 during the different combustion cases.

3.2. Laser transmission and signal formation

The TDLAS+CPFAAS system was set to Port 2 to monitor whether KCl remains intact or is dissociated in the flame after the injection. As expected in the temperature of 1750 °C and in fuel-rich conditions, the KCl dissociated into atomic potassium to the extent that the flame was completely opaque for the near-infrared potassium probe beam across the tuning range already when the KCl seeding was only 10 ppm. Therefore, no quantitative information was obtained from Port 2. The flame remained opaque also during simultaneous KCl and SO_2 injection.

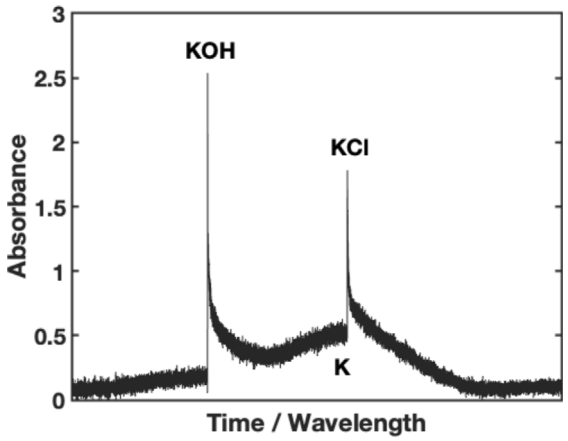

Fig. 4. An example of a measured single shot absorbance by the TDLAS+CPFAAS system. The *x*-axis is measured as time but can be converted into wavelength for atomic potassium absorption line fitting using the lineshape obtained with reference potassium cell transmittance that has well known characteristics.

As mentioned, the visual flame tip fluctuated between Port 5 and Port 6 or remained above the Port 6 level in case of OF25. Thus, the interaction length between the atomic potassium in the flame and the probe beam would be shorter in these ports enabling lower probe beam absorption and, consequently, quantitative potassium species detection. Indeed, during KCl injection aimed for 10 ppm to 100 ppm in the flue gas, the observed absorbance was favorable for quantitative potassium species detection in Ports 5, 6 and 7 for OF25 conditions and in Ports 6 and 7 for Air case.

The example single shot absorbance curve in Fig. 4 is collected during Air combustion case with TDLAS+CPFAAS through Port 6. The potassium probe laser beam is wavelength modulated over time and, therefore, the x-axis of collected TDLAS+CPFAAS signals can represent time or wavelength. The probe beam wavelength was monitored utilizing transmission signal through the reference potassium cell that enabled, firstly, locating the correct wavelength for potassium detection, and, secondly, provides a reference for the time-to-wavelength axis conversion as the reference lineshape and width is well known. The threshold for the probe beam absorbance saturation, i.e., when the probe beam transmission goes to zero in the peak of the absorption line, in propagation through the unit is approximately 5 ppb. Qu et al. have demonstrated a method to quantify atomic alkali species also in thick optical conditions [14]. However, especially in Port 5 and, during air combustion, also in Port 6, the flame fluctuation caused occasionally the transmission to drop to zero across the whole wavelength range and no quantitative information could be obtained from these signals. Despite the N_2 flushing, the windows in port inlets suffered from fine deposition over the seeding period that could be seen as a shift in the frequency-dependent interference fringes in the signal. Thus, to reduce the uncertainty in quantification of the atomic potassium and determination of the potassium lineshape parameters, the I_0 signal was measured switching the injected solution to water and recording the temporal transmission signal immediately after the switch when no potassium species were observed.

The potassium absorption lineshape was observed to vary between the port locations and combustion cases. Therefore, the potassium absorption lineshape parameters for wavelength dependent absorption cross sections in KCl and KOH quantification were validated separately for Ports 5, 6, and 7 in all combustion cases. As no atomic potassium was detected in Port 7 during KCl injection, KNO_3 solution was injected into the unit instead. Theoretical injection of 30 ppm of KNO_3 produced atomic potassium concentration of 3 ppb to the Port 7 level enabling validation of the potassium lineshape in Port 7. As the temperature distribution in Port 7 is almost flat with little variation between the proximity of the wall and the center of the unit, the obtained wavelength dependent absorption cross section curve for KCl quantification in Port 7 can be considered to hold across the unit diameter. On the other hand, the absence of atomic potassium enabled the detection of KCl in the proximity of the absorption peak similarly to fixed wavelength CPFAAS [25] that has shown to have low variation in fragmented potassium absorption section across wide temperature range, thus, further reducing the uncertainty in the potassium absorption cross section. In addition, the obtained KCl values agreed well with SID values that were independently calibrated, as will be shown in Section 3.3. In Port 6 for Air case and in Port 5 for OF25 case, the temperature distribution cause uncertainty to the KCl and KOH quantification as the potassium lineshape is obtained from the center of the unit that is in higher temperature than the outer gas layers. This may lead to underestimation of the KCl concentration as KCl is typically met in lower temperatures than atomic potassium or KOH. However, the obtained KCl concentrations were close to the theoretical maximums and, thus, no clear underestimations were observed.

3.3. Potassium detection during sulfation

The ability to track the gas phase reactions of the potassium species is demonstrated by measuring the evolution of the K, KOH, and KCl fractions during sulfation process at different distances from the burner. The K, KCl and KOH concentration values shown in Table 2 are averaged over 500 individual signals and, thus, the values represent 50 s of the unit operation. The aimed KCl seeding for the sulfation tracking in gas phase was chosen to be 10 ppm as it enabled 50 s long signal acquisition without complete loss of probe beam transmission in all measurement ports used. In higher KCl seeding conditions, occasionally the fluctuating flame and resulting transmission loss caused higher uncertainty to the obtained data. It is worth to notice that the atomic potassium and KOH are not evenly distributed along the measurement volume but concentrated to the central part of the reactor. Hence, the local concentrations of atomic potassium and KOH can be substantially higher than the obtained line-of-sight values. Based on the KCl concentrations obtained at Port 6 and Port 7 levels, the most efficient sulfation during air combustion occurs between Ports 6 and 7. In case of OF25, sulfation was observed already at Port 6 as the temperature had reduced to a level that favors alkali sulfation [32]. In addition, the S/K ratio was higher during OF25 which also promotes KCl sulfation as shown by Ekvall et al. in Ref. [24] that includes a numerical study on the sulfation occurring in the same unit with the parameters used in this work.

The current laser measurement system can deliver data on potassium species concentration with temporal resolution of up to 10 Hz. The sulfation behavior of the potassium species K, KOH, and KCl was observed during the initiation of SO_2 injection with the aim to see how species are affected by fast transient of the SO_2 concentration. As can be seen in Table 2, the atomic potassium concentration was not affected within the dynamic range of the atomic potassium detection by the SO_2 injection and the same was observed in temporally resolved concentration curves. The obtained atomic potassium signal was heavily saturated despite the SO_2 injection. This was expected as the atomic potassium was mainly located in the areas with temperatures exceeding 1000 °C that is not favorable for alkali sulfation in reducing conditions [33]. To study the sulfation details of atomic potassium in pilot-scale facilities, an extension to the dynamic range of atomic potassium detection could be obtained using potassium D1 line instead of the potassium D2 line for the atomic potassium detection [14].

Example curves of KCl and KOH measured in Port 6 during the Air combustion case are shown in Fig. 5a, where the single shot concentration data is averaged over 0.5 s intervals. The KCl and KOH levels were not affected by the SO_2 injection at Port 6 level during Air combustion case even at the S/K ratio of 60 that is the highest obtained in this study. When the temporal concentrations were observed in Port

Table 2
The average concentrations of potassium species during the different combustion cases in Port 5, 6 and 7. The values are averaged over 50 s of combustion unit operation and represent the averaged amount along the unit diameter.

Case	Air						OF25					
S/K	0			30			0			98		
	K (ppb)	KCl (ppm)	KOH (ppm)	K (ppb)	KCl (ppm)	KOH (ppm)	K (ppb)	KCl (ppm)	KOH (ppm)	K (ppb)	KCl (ppm)	KOH (ppm)
Port 5							>5	–	0.4 ± 0.2	>5	–	0.5 ± 0 – 2
Port 6	>5	9 ± 4	0.1 ± 0.1	≥5	8 ± 4	0.1 ± 0.1	–	12 ± 1	0.2 ± 0.1	–	5 ± 2	0.1 ± 0.1
Port 7	–	12 ± 3	–	–	3 ± 3	–	–	7 ± 2	–	–	–	–

Table 3
Comparison values at Port 7 level obtained by SID and CPFAAS during different seeding cases.

Alkali salt (ppm)	KCl (100)			KCl (50)+NaCl (50)		
S/K	0	3	6	0	6	12
CPFAAS [KCl] (ppm)	89	51	29	54	35	20
SID $[KCl]_{eq}$ (ppm)	80	51	32	79	57	37

7, as shown in Fig. 5b, a rapid response in KCl concentration was obtained after initiation of SO_2 injection at t = 0 s. Complete sulfation in the limits of the LoD was observed already at S/K = 30. This further demonstrates that there is efficient sulfation between the Ports 6 and 7. The region between the Ports 6 and 7 is in the post-flame zone where the temperature is reduced from 950 °C to around 800 °C. The strong temporal fluctuation in Fig. 5a arise mainly from the proximity of the LoD and the reduced certainty in the fitting procedure. Proximity of the fluctuating flame may also contribute to the temporal behavior of the alkali elements. The fluctuations in KCl concentration also increased when the KCl injection was increased to 100 ppm as can be seen in Fig. 5c. This might be due to the alkali induced fluctuations in the combustion behavior, however, this will be a topic of another study.

The transient response of KCl concentration to SO_2 injection was studied with different S/K ratios. Fig. 5b shows the KCl response in three of the S/K cases in Port 7 level. The rate of sulfation is quite similar for all tested ratios, however, the steady state levels differ. In Fig. 5c it is shown one more S/K ratio and a seeding case where 50% of the KCl is replaced with NaCl, i.e. the sulfur-to-alkali ratio (S/A) is the same in both cases but S/K ratio is doubled. Again, the response rate is very similar but interestingly the KCl concentration after initiation of SO_2 injection, when the system has reached the steady state, is the same in both cases with target concentrations of 100 ppm in alkali content in the flue gas. This observation suggests that sulfation of NaCl is favored over KCl sulfation leaving behind higher KCl level than an equal rate of sulfation would contribute. However, more measurements with a matrix of different S/K and S/A ratios is required to confirm this observation.

The responses of the laser diagnostic system and SID method were compared during the KCl sulfation process. The laser propagation path and the SID sampling point are at the same distance from the burner at Port 7 level and approximately 3 cm apart in the middle of the reactor. To compare the quantitative alkali concentration values between the laser system and the SID, the reactor was seeded with different alkali solutions aiming to have a KCl-equivalent concentration of 100 ppm in the flue gas during air combustion. In addition, three different SO_2 concentrations, 0 ppm, 300 ppm, and 600 ppm, were introduced. The results are summarized in Table 3. When seeding 100 ppm of KCl, the quantitative KCl concentration values from SID and CPFAAS agree well with 80.1 ppm and 88.5 ppm, respectively. The KCl concentration is reduced in the gas phase when SO_2 is introduced to the combustion gas, as can be seen in the CPFAAS KCl concentration. The obtained SID signal is reduced as well due to the SID method's lower response to K_2SO_4 molecules [30]. The simultaneous injection of KCl and NaCl shows the benefit of two complementing methods as the other one tells the total alkali content in the flue gas and the other provides

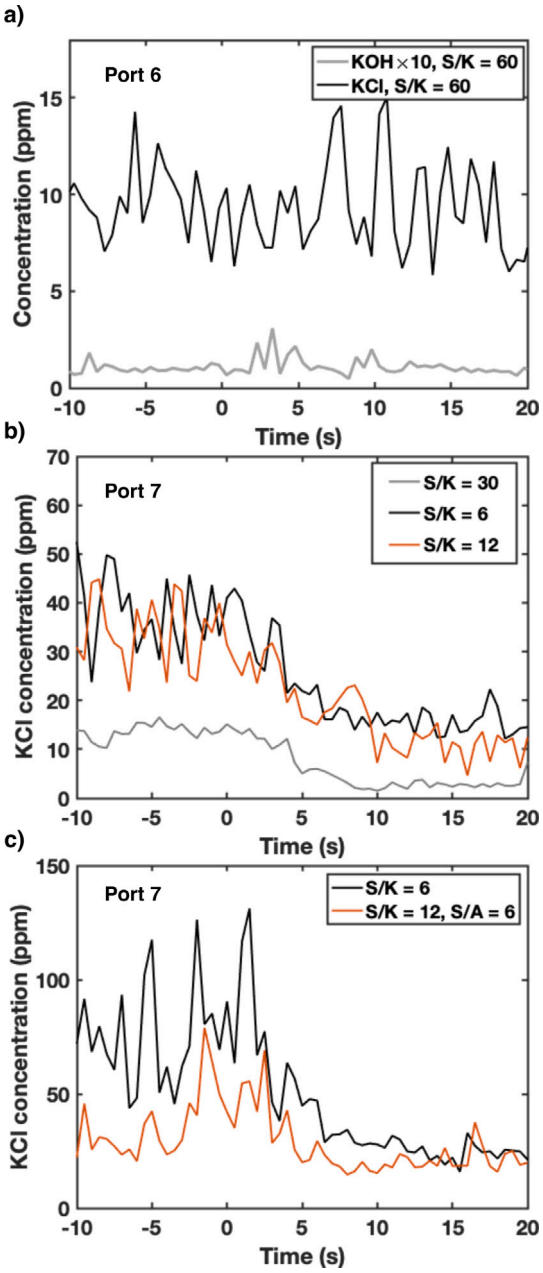

Fig. 5. (a) Transient KCl and KOH concentrations at Port 6 level, (b) transient KCl concentration in gas phase at Port 7 in case of different K/S ratios, and (c) KCl concentration in gas phase at Port 7 level in equal S/Alkali ratios but different amounts of potassium during initiation of SO_2 injection at t = 0 s in the case of air combustion.

information on the selected species. The sulfation process creates a challenge for species identification and alkali quantification also for the parallel systems introduced in this work. If the KCl + NaCl seeding case

Table 4
The overall combustion conditions and SID and CPFAAS measured KCl concentrations during the four different load cases investigated in this work. Load 1 is equal to the Air combustion case. The temperature is defined using the CPFAAS signal recovery curve [34].

Load case	Load 1	Load 2	Load 3	Load 4
Thermal input (kW)	80	62	29	29
Oxygen-to-fuel ratio	1.15	1.22	2.24	1.37
Residence time (s)	4.4	6.1[a]	7.7[a]	13.2[a]
Theoretical KCl (ppm)	100	124	149	237
Measurement results				
SID $[KCl]_{eq}$ (ppm)	90	94	131	182
CPFAAS [KCl] (ppm)	101	61	7	3
Temperature (°C)	859	731	670	600

[a]Estimated from volumetric flow and obtained temperature values.

with SO_2 seeding cases shown in Table 3 would be an unknown flue gas sample, the interpretation of the results would be difficult and cause uncertainties without additional measurement data from, e.g., FTIR on SO_2 content in flue gas.

3.4. Detection of homogeneous alkali nucleation

To demonstrate the possibility to study the KCl phase transition from vapor to particles, the unit load and, consequently, temperature was stepwise decreased, while keeping the KCl seeding constant. The laser-detected KCl concentration in gas phase decreased from 100 ppm to 3 ppm during the load ramp down. Simultaneously, the observed SID signal increased as the total alkali concentration increased in the flue gas due to the reduced volumetric gas flow in the unit, as shown in Table 4 as increased residence time. The KCl vapor temperature was analyzed using the recovery of the CPFAAS transmission signal after the fragmentation pulse [34]. The vapor temperature also showed a decreasing trend as the load was reduced. The reduction in temperature below 750 °C coincides with the beginning of the substantial reduction of gas phase KCl concentration. Simultaneously, the KCl-equivalent alkali concentration obtained with SID remained persistent and started to increase with reduction in the volumetric flow through the unit as the KCl seeding remained constant. The losses in KCl-equivalent concentration compared to the theoretical seeding increased in lower load cases presumably due to the increased KCl deposition to the unit cooling rods as the result of the lower volumetric flow and coinciding increased residence time. However, the SID suffered from dilution problems during the ramp down experiment and, therefore, the uncertainty in this experiment is higher than previously reported 2.5% [30].

The obtained particle size distribution, given in Fig. 6, shifts during the load reduction. Initially, at higher load, the particle size distribution show two distinct modes around particle diameters of 30 and 140 nm, respectively. These modes are typically observed during fresh nucleation of a supersaturated vapor, as when the high alkali containing sample gas is rapidly cooled with cold dilution gas. As the burner load is reduced the size distribution shifts towards larger particles, towards a so-called accumulation mode, where nucleated particles have grown by condensation and impaction suggesting that the particles are formed prior to the sampling. The reduction of the burner load coincides well with decreased gas species concentration, increased SID mass concentration, and a shift in observed aerosol size distribution.

The temperature dependence of KCl nucleation was modeled in FactSage 7.2 software to interpret the results further. This model assumes global thermodynamic equilibrium, predicting thermodynamically stable species based on Gibbs free energy minimization in a mass balance constrained system. The model assumes ideal mixing and is not constrained by mass transport or chemical reaction kinetics. The FactSage model used FactPS database for thermodynamic properties of the reacting components and was run at temperature increments of

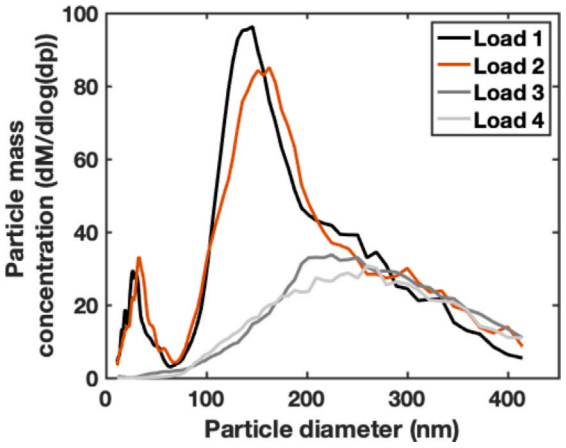

Fig. 6. The evolution of detected particle size distribution during load ramp-down.

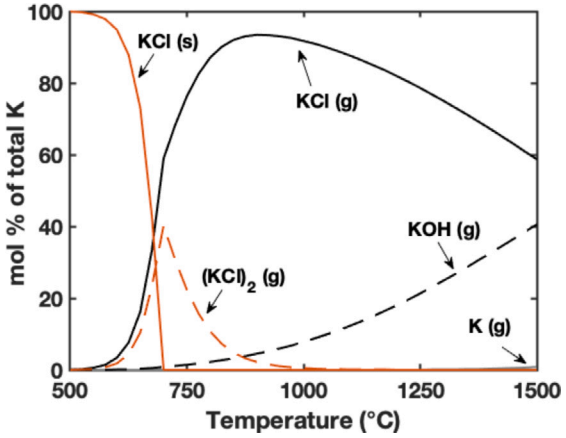

Fig. 7. The mol% of total potassium as function of temperature modeled using FactSage software.

25 °C in the range from 500–1500 °C, corresponding to the temperature range of the reactor. The obtained mol% fractions of total potassium content are shown in Fig. 7. The nucleation model agrees well with the previously presented models [10,12] and the observations in the current study. The transition from Load 1 to Load 2 reduced the flue gas temperature to 730 °C and did not cause significant difference in the total KCl equivalent value obtained by SID nor in particle size distribution. However, substantial reduction of 40% in KCl vapor was observed with the laser diagnostics. This reduction is equivalent to the modeled formation of gaseous $(KCl)_2$ dimers that are not visible for the laser diagnostics and do not cause significant changes in the SID and in the particle size distribution signals. As the load was further lowered, the KCl vapor temperature in flue gas reduced to 670 °C and caused substantial changes in the particle size distribution and reduction of gas phase KCl. The distribution shifted towards larger particles and the nucleation mode disappeared indicating that the particles were formed prior the sampling. The FactSage model agrees with the observations during the load ramp down from Load 2 to Load 3 showing that the temperature crosses the point where homogeneous nucleation occur and the main fraction of KCl is transformed from gas phase to solid phase.

The agreement of the FactSage model and the obtained measurement results with parallel measurement systems are strong evidence that we observe a precise temperature threshold where nucleation appears. Nucleation front and nucleation events are typically challenging to study, however, in the present study we have been able to follow this process in a pilot-scale combustion environment. Furthermore, the

work demonstrates how simultaneous use of in-situ laser diagnostics for monitoring the gas phase potassium behavior and SID for total alkali content monitoring in flue gas flow are required to obtain more complete picture of the alkali behavior in dynamic industrial-scale combustion applications. SID measurements rely on extractive sampling and, thus, cannot distinguish whether the detected alkali signal originates from primary particles or particles formed during extraction and conditioning. Closer inspection on detected particle size distribution could help in the recognition, however, this approach is case specific and depends on the extraction system. On the other hand, optical in-situ gas phase detection of selective species may omit information about alkali species content during operational changes that are becoming more and more common due to the heterogeneous fuels and increasing dynamics of the power grid [35]. In addition, demonstration of the laser measurement system in oxy-fuel conditions is a powerful statement of the method's abilities in various combustion conditions. Thus, the use of parallel alkali measurement systems introduced in this work opens multiple research lines.

4. Conclusion

A combination of methods that can follow alkali species from vapor to particles in a pilot-scale combustor is introduced. The laser-based in-situ measurement technique TDLAS+CPFAAS enable monitoring of K, KCl, and KOH in different stages of the combustion and is here demonstrated for various combustion conditions: Air and OF25. The SID is capable to detect the total alkali content in the gas phase and in freshly formed particles providing additional insight on the faith of the alkali species, thus, providing complementing information for selective gas phase data obtained with laser diagnostics. Heterogeneous fuel qualities and dynamic power grid have become more and more common, therefore, information of alkali behavior in highly dynamic environments is desired. Utilizing the combination of in-situ laser methods and the SID, we demonstrate continuous alkali monitoring during load ramping and show the movement of the KCl nucleation zone along the unit axis. The critical temperature where the nucleation occurs was shown to be approximately 700 °C that agrees well with the FactSage model. The ability to observe potassium dynamics in gas phase and in solid phase in varying combustion conditions enable vast selection of future studies and experiments that can clarify the alkali behavior in high-temperature processes.

CRediT authorship contribution statement

Jan Viljanen: Investigation, Methodology, Writing – original draft, Conceptualization. **Dan Gall:** Investigation, Methodology, Writing – original draft. **Ivan Gogolev:** Methodology, Writing – review and editing. **Thomas Allgurén:** Investigation, Conceptualization, Writing – original draft. **Klas Andersson:** Supervision, Validation, Funding acquisition.

Declaration of competing interest

The authors declare that they have no known competing financial interests or personal relationships that could have appeared to influence the work reported in this paper.

Data availability

Data will be made available on request.

Acknowledgments

This work was supported by the Swedish Energy Agency, Sweden (project 44887-1). J.V. acknowledges the grant by Academy of Finland, Finland (decision 338338).

References

[1] Agency IE. Global energy review 2020. OECD Publishing; 2020.
[2] Zhou H, Zhou B, Li L, Zhang H. Experimental measurement of the effective thermal conductivity of ash deposit for high sodium coal (Zhun Dong coal) in a 300 KW test furnace. Energy Fuels 2013;27(11):7008–22.
[3] Glarborg P. Hidden interactions—Trace species governing combustion and emissions. Proc Combust Inst 2007;31(1):77–98.
[4] McKee DW. Mechanisms of the alkali metal catalysed gasification of carbon. Fuel 1983;62(2):170–5.
[5] Hupa M, Karlström O, Vainio E. Biomass combustion technology development–It is all about chemical details. Proc Combust Inst 2017;36(1):113–34.
[6] Johansen JM, Jakobsen JG, Frandsen FJ, Glarborg P. Release of K, Cl, and S during pyrolysis and combustion of high-chlorine biomass. Energy Fuels 2011;25(11):4961–71.
[7] Thorin E, Zhang K, Valiev D, Schmidt FM. Simultaneous detection of K, KOH, and KCl in flames and released from biomass using photofragmentation TDLAS. Opt Express 2021;29(26):42945–61.
[8] Weng W, Chen S, Wu H, Glarborg P, Li Z. Optical investigation of gas-phase KCl/KOH sulfation in post flame conditions. Fuel 2018;224:461–8.
[9] Hu Z, Wang X, Zhou Y, Wu H, Glarborg P, Tan H. Assessment of the effect of alkali chemistry on post-flame aerosol formation during oxy-combustion of biomass. Fuel 2022;311:122521.
[10] Jensen JR, Nielsen L, Schultz-Møller C, Wedel S, Livbjerg H. The nucleation of aerosols in flue gases with a high content of alkali-A laboratory study. Aerosol Sci Technol 2000;33(6):490–509.
[11] Christensen KA, Livbjerg H. A plug flow model for chemical reactions and aerosol nucleation and growth in an alkali-containing flue gas. Aerosol Sci Technol 2000;33(6):470–89.
[12] Christensen KA, Stenholm M, Livbjerg H. The formation of submicron aerosol particles, HCl and SO2 in straw-fired boilers. J Aerosol Sci 1998;29(4):421–44.
[13] Monkhouse P. On-line spectroscopic and spectrometric methods for the determination of metal species in industrial processes. Prog Energy Combust Sci 2011;37(2):125–71.
[14] Qu Z, Steinvall E, Ghorbani R, Schmidt FM. Tunable diode laser atomic absorption spectroscopy for detection of potassium under optically thick conditions. Anal Chem 2016;88(7):3754–60.
[15] Schlosser E, Fernholz T, Teichert H, Ebert V. In situ detection of potassium atoms in high-temperature coal-combustion systems using near-infrared-diode lasers. Spectrochimi Acta A 2002;58(11):2347–59.
[16] Forsberg C, Broström M, Backman R, Edvardsson E, Badiei S, Berg M, Kassman H. Principle, calibration, and application of the in situ alkali chloride monitor. Rev Sci Instrum 2009;80(2):023104.
[17] Sorvajärvi T, Saarela J, Toivonen J. Optical detection of potassium chloride vapor using collinear photofragmentation and atomic absorption spectroscopy. Opt Lett 2012;37(19):4011–3.
[18] Viljanen J, Allgurén T, Wang Y, Li X, Toivonen J, Andersson K, Wendt JO. In-situ monitoring of transient gas phase K–Cl–S chemistry in a pilot-scale combustor. Proc Combust Inst 2021;38(1):1823–31.
[19] Thorin E, Sepman A, Ögren Y, Ma C, Carlborg M, Wennebro J, Broström M, Wiinikka H, Schmidt FM. Quantitative real-time in situ measurement of gaseous K, KOH and KCl in a 140 kW entrained-flow biomass gasifier. Proc Combust Inst 2022.
[20] Davidsson KO, Engvall K, Hagström M, Korsgren JG, Lönn B, Pettersson JB. A surface ionization instrument for on-line measurements of alkali metal components in combustion: Instrument description and applications. Energy Fuels 2002;16(6):1369–77.
[21] Gogolev I, Soleimanisalim AH, Linderholm C, Lyngfelt A. Commissioning, performance benchmarking, and investigation of alkali emissions in a 10 kWth solid fuel chemical looping combustion pilot. Fuel 2021;287:119530.
[22] Gall D, Pushp M, Larsson A, Davidsson K, Pettersson JB. Online measurements of alkali metals during start-up and operation of an industrial-scale biomass gasification plant. Energy Fuels 2018;32(1):532–41.
[23] Andersson K, Johnsson F. Flame and radiation characteristics of gas-fired O2/CO2 combustion. Fuel 2007;86(5–6):656–68.
[24] Ekvall T, Andersson K, Leffler T, Berg M. K–cl–s chemistry in air and oxy-combustion atmospheres. Proc Combust Inst 2017;36(3):4011–8.
[25] Sorvajärvi T, DeMartini N, Rossi J, Toivonen J. In situ measurement technique for simultaneous detection of K, KCl, and KOH vapors released during combustion of solid biomass fuel in a single particle reactor. Applied Spectrosc 2014;68(2):179–84.
[26] Sorvajärvi T, Toivonen J. Principles and calibration of collinear photofragmentation and atomic absorption spectroscopy. Appl Phys B 2014;115(4):533–9.
[27] Sorvajärvi T, Viljanen J, Toivonen J, Marshall P, Glarborg P. Rate constant and thermochemistry for K+ O_2+ N_2=KO_2+ N_2. J Phys Chem A 2015;119(14):3329–36.
[28] Holmlid L, Olsson JO. Molecular beam surface ionization detection: I. Absolute ionization coefficients and work function of low work function pt (8% W) surfaces. Surf Sci 1976;55(2):523–44.

[29] Andersson L, Olsson J, Holmlid L. Surface ionization at atmospheric pressure: partial melting of alkali salt particles. Langmuir 1986;2(5):594–9.
[30] Gall D, Viljanen J, Gogolev I, Allgurén T, Andersson K. Alkali monitoring of industrial process gas by surface ionization - calibration, assessment, and comparison to in situ laser diagnostics. Energy Fuels 2021;35(24):20160–71.
[31] Jiménez S, Ballester J. A comparative study of different methods for the sampling of high temperature combustion aerosols. Aerosol Sci Technol 2005;39(9):811–21.
[32] Schmid D, Weng W, Li S, Karlström O, Hupa M, Li Z, Glarborg P, Marshall P, Aldén M. Optical in-situ measurements and modeling of post-flame sulfation of NaOH (g) and naCl (g). Fuel 2023;332:126337.
[33] Allgurén T, Viljanen J, Li X, Wang Y, Andersson K, Wendt JO. Alkali sulfation during combustion of coal in a pilot scale facility using additives to alter the global sulfur to potassium and chlorine to potassium ratios. Proc Combust Inst 2021;38(3):4171–8.
[34] Viljanen J, Sorvajärvi T, Toivonen J. In situ laser measurement of oxygen concentration and flue gas temperature utilizing chemical reaction kinetics. Opt Lett 2017;42(23):4925–8.
[35] Smith O, Cattell O, Farcot E, O'Dea RD, Hopcraft KI. The effect of renewable energy incorporation on power grid stability and resilience. Sci Adv 2022;8(9):eabj6734.